Electronic Supplementary Information

A crown ether embedded responsive π-gelator for transition from one-component gel to two-component gel

Simei Wu, Wei Tao, Tao Wang, Jieqiong Xu* and Peifa Wei*

Anhui Graphene Engineering Laboratory, Key Laboratory of Structure and Functional Regulation of Hybrid Materials of Ministry of Education, Institutes of Physical Science and Information Technology, Anhui University, Hefei, Anhui 230039, China

***Authors to whom correspondence should be addressed:** pfwei@ahu.edu.cn (P. Wei); jieqiongxu@ahu.edu.cn (J. Xu)

Table of Contents

1. Experimental Section

1.1 Materials and Characterization

All reagents were commercially available and used as supplied without further purification. Solvents were either employed as purchased or dried according to procedures described in the literature[1]. NMR spectra were recorded on a Bruker Advance DMX 400 MHz spectrophotometer with deuterated solvent as the lock. Chemical shifts were reported relative to residual solvent signals. High-resolution mass spectra were obtained on a Finnigan MAT TSQ 7000 Mass Spectrometer operated at ESI Ion source. Absorption spectra were recorded on a UV-Vis Spectrophotometer U-3900 spectrophotometer. Photoluminescence spectra was recorded on a spectrofluorometer FS 5. Fluorescent microscopy images were acquired at an excitation wavelength of 365 nm using a Nikon Ni-U Fluorescence Microscope equipped. The lifetime was measured on a Horiba Fluoro max plus equipped with a xenon arc lamp (Xe900). The absolute fluorescence quantum yields were recorded on a Fluormax-4P spectrometer. Scanning electron microscopy (SEM) images were collected on a Hitachi Regulus 8230 SEM. The X-ray diffraction (XRD) patterns of all as-prepared samples were collected by X-ray diffractometer (Japan Rigaku D/MAX-γA) with Cu-Kα radiation (λ = 0.154 nm). The crystal data were collected on a Stoe Stadivari instrument. The photoreaction was carried out under irradiation from a 365 nm hand-held UV lamp (1.67 $W \cdot cm^{-2}$).

1.2 Synthesis of compound 1

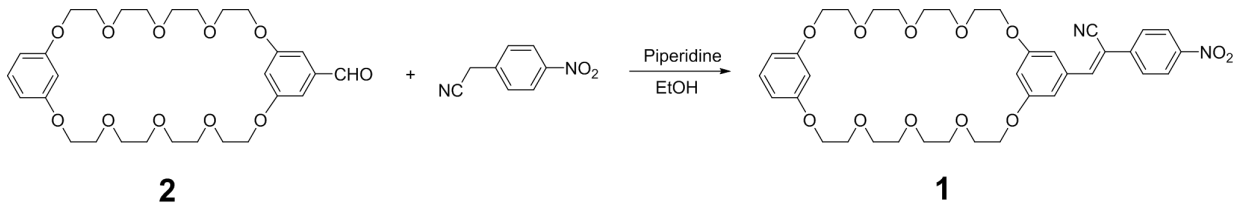

Scheme S1. Synthetic route of **1.**

Compound **2**[2] (0.2 g, 0.35 mmol) was mixed with *p*-nitrophenylacetonitrile (0.069 g, 0.42 mM) in ethanol (5 mL). Piperidine (0.15 mL) was added and the solution became berry red. The solution was heated to reflux for 3 h. The mixture was purified by column chromatography (dichloromethane/methanol mixture, 200:1 *v*/*v*) to afford compound **1**. The ^{1}H NMR spectrum of **1** was shown in Figure S1. ^{1}H NMR (CD_3OD, 298 K, 400 MHz), δ (ppm): 8.32-8.34 (d, 2H), 7.94-7.96 (d, 2H), 7.90 (s, 1H), 7.17 (s, 2H), 7.02-7.06 (t, 1H), 6.66 (s, 1H), 6.43-6.45 (d, 2H), 6.40 (s, 1H), 4.12-4.14 (m, 4H), 3.99-4.01 (m, 4H), 3.84-3.87 (t, 4H), 3.80-3.82 (t, 4H), 3.68-3.71 (d, 16H). The ^{13}C NMR spectrum of **1** was shown in Figure S2. ^{13}C NMR ($CDCl_3$, 298 K, 400 MHz), δ (ppm): 160.39, 160.09, 148.02, 145.79, 140.68, 134.48, 129.89, 126.93, 124.45, 117.30, 109.71, 108.56, 107.22, 105.64, 101.80, 71.04, 71.00, 69.83, 69.68. HRMS (Figure S3): *m/z* calcd for $[M + H]^+$ $C_{37}H_{45}N_2O_{12}$ 709.2972; found 709.2927.

1.3 Synthesis of compound M1

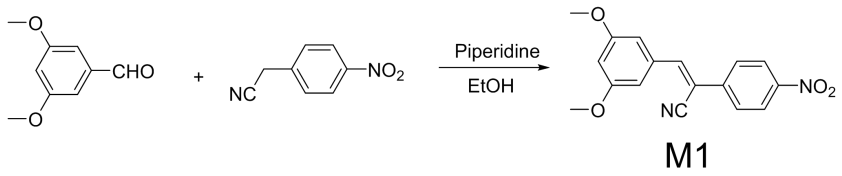

Scheme S2. Synthetic route of M1.[2]

3,5-dimethoxybenzaldehyde (0.10 g, 0.60 mmol) was mixed with *p*-nitrophenylacetonitrile (0.081 g, 0.50 mmol) in ethanol (10.0 mL). Piperidine (0.20 mL) was added and the solution

became berry red. The solution was stirred at room temperature for 3 h, then a yellow solid mixture was obtained. The reaction mixture was filtered, the residue was washed with ethanol to afford compound M1 as a yellow solid. The ^{1}H NMR spectrum of M1 was shown in Figure S7. ^{1}H NMR (DMSO-d_6, 298 K, 400 MHz), δ (ppm): 8.38 (s, 1H), 8.35-8.36 (d, 1H), 8.25 (s, 1H), 8.04-8.05 (d, 1H), 8.03 (s, 1H), 7.21 (dd, 2H), 6.71-6.72 (t, 1H), 3.82 (s, 6H).

1.4 Synthesis of compound M2

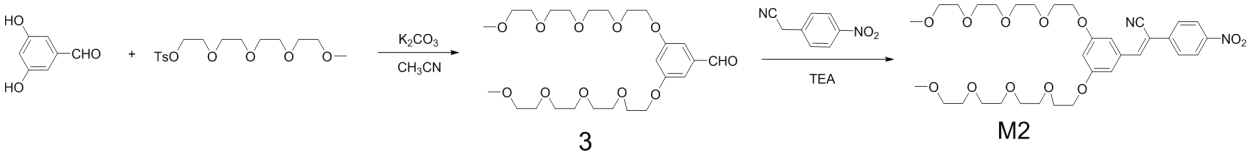

Scheme S3. Synthetic routes of M2**.**

3,5-dihydroxybenzaldehyde (0.22 g, 1.62 mmol) was mixed with 2,5,8,11-tetraoxatridecan-13-yl 4-methylbenzenesulfonate (1.18 g, 3.26 mmol) in acetonitrile (40 mL). Potassium carbonate (0.90 g, 6.54 mmol) was added and the solution were heated to reflux for 48 h under nitrogen atmosphere. The solution turned brown and the mixture was purified by column chromatography (ethyl acetate) to afford compound **3**.[3] *P*-nitrophenylacetonitrile (0.16 g, 1.01 mmol) was added into a solution of compound **3** (0.44 g, 0.85 mmol) in ethanol (20 mL). Triethylamine (0.17 g, 1.67 mmol) was added and the solution became berry red. The mixture was heated to reflux. After 8 h, a green reaction mixture was obtained. The mixture was purified by column chromatography (ethyl acetate/petroleum ether mixture, 2:1 *v*/*v*) to afford compound M2. The ^{1}H NMR spectrum of M2 was shown in Figure S8. ^{1}H NMR ($CDCl_3$, 298 K, 400 MHz), δ (ppm): 8.30-8.32 (d, 2H), 7.83-7.85 (d, 2H), 7.58 (s, 1H), 7.10 (d, 2H), 6.65-6.66 (t, 1H), 4.16-4.18 (m, 4H), 3.87-3.88 (m, 4H), 3.70-3.74 (m, 4H), 3.63-3.69 (m, 16H), 3.54-3.55 (m, 4H), 3.37 (s, 6H). The ^{13}C NMR spectrum of M2 was shown in Figure S9. ^{13}C NMR ($CDCl_3$, 298 K, 400 MHz), δ (ppm): 160.35, 148.04, 145.72, 140.64, 134.51, 126.93, 129.89, 124.46, 117.27, 109.86,

108.45, 105.68, 72.03, 70.94, 70.72, 70.62, 69.66, 67.91. HRMS (Figure S10): *m/z* calcd for [M + H]$^+$ $C_{33}H_{47}N_2O_{12}$ 663.3129; found 663.3120.

1.5 Synthesis of compound PQD

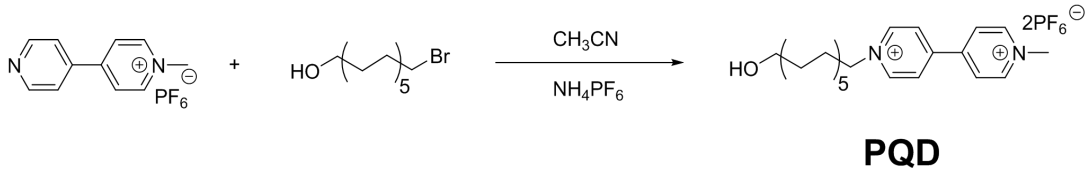

Scheme S4. Synthetic route of **PQD.**[2]

1-methyl-4-phenylpridinium hexafluorophosphate (0.32 g, 1.00 mmol) was added into a solution of 12-bromo-1-dodecanol (0.17 g, 1.10 mmol) in acetonitrile (40 mL). The mixture was heated to reflux. After 24 h, the yellow precipitate formed and it was collected by suction filtration and washed with acetonitrile. Then saturated aqueous NH_4PF_6 solution was added into the solution of the product dissolved in methanol. The mixture was stirred at room temperature for 6 h, then a white solid mixture was obtained. The precipitate was collected by suction filtration and washed with deionized water to afford compound PQD as a white solid. The ^{1}H NMR spectrum of PQD was shown in Figure S19. ^{1}H NMR ($CDCl_3$, 298 K, 400 MHz), δ (ppm): 8.83-8.89 (dd,4H), 8.35-8.38 (t, 4H), 4.59-4.62 (t, 2H), 4.40 (s, 3H), 3.44-3.49 (m, 2H), 2.41-2.44 (t, 1H), 1.99-2.04 (m, 2H), 1.44-1.48 (t, 2H), 1.29-1.37 (d, 16H).

1.6 Preparation of gel 1 and gel 1⊃PQD.

The gel **1** was prepared by dissolving **1** in methanol (or DMSO and DMF) with gentle heating (1.73 wt% in methanol; 2.46 wt% in DMF; 2.53 wt% in DMSO), followed by slow cooling to room temperature. Then the gel **1** formed after cooling of sol **1**. As expected, gel **1⊃PQD** was formed in organic solution similar with gel **1**. Firstly, **1** and PQD mixture were

added to methanol (10.21 wt%), then gently stirred and heated to disperse them. After cooling to room temperature, a two-component co-assembly gel **1⊃PQD** was obtained.

1.7 Preparation of crystal 1 and crystal 1c.

Both crystal **1** and crystal **1c** were prepared through the vapor diffusion method. Firstly, **1** powder was dissolved in methanol in a 3 ml bottle. Then, placed it in a 20 ml bottle with cyclohexane in a 4 °C refrigerator. After 2 days, the pale-yellow acicular crystal blanketed the bottom of the 3 ml bottle. The preparation procedure of crystal **1c** was similar with crystal **1**, and the slight difference was that crystal **1c** grew in acetonitrile/isopropyl ether system.

1.8 ^{1}H NMR titration test of 1⊃PQD.

^{1}H NMR titrations were done with solutions which had a constant concentration of **1** (1.00 mM) and varying concentrations of PQD. By a nonlinear curve-fitting method, the association constant between PQD and **1** was calculated. Treatment of the collected ^{1}H NMR data with a non-linear curve-fitting program afforded the corresponding K_a: (299.4 ± 16) M^{-1} for **1**⊃PQD. The non-linear curve-fitting was based on the equation:

$$\Delta\delta = (\Delta\delta_\infty/[\mathbf{1}]_0)\,(0.5[\mathrm{PQD}]_0 + 0.5([\mathbf{1}]_0 + 1/K\mathrm{a}) - (0.5\,([\mathrm{PQD}]_0^2 + (2[\mathrm{PQD}]_0(1/K\mathrm{a} - [\mathbf{1}]_0)) + (1/K\mathrm{a} + [\mathbf{1}]_0)^2)^{0.5})) \quad \text{(Eq. S1)}$$

Where $\Delta\delta$ is the chemical shift change of H_σ on **1** at $[\mathbf{1}]_0$, $\Delta\delta_\infty$ is the chemical shift change of **1** when PQD is completely complexed, $[\mathbf{1}]_0$ is the fixed initial concentration of **1**, and $[\mathrm{PQD}]_0$ is the varying concentrations of PQD.

2. Results and Discussion

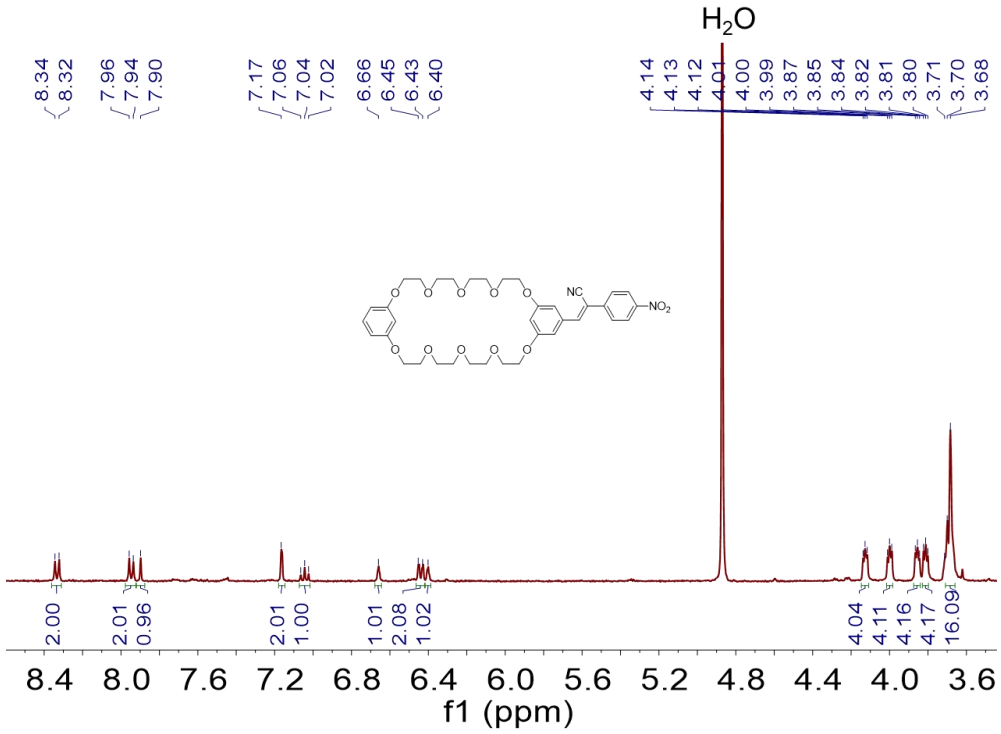

Fig. S1. The ^{1}H NMR spectrum (400 MHz, CD_3OD, 298 K) of **1**.

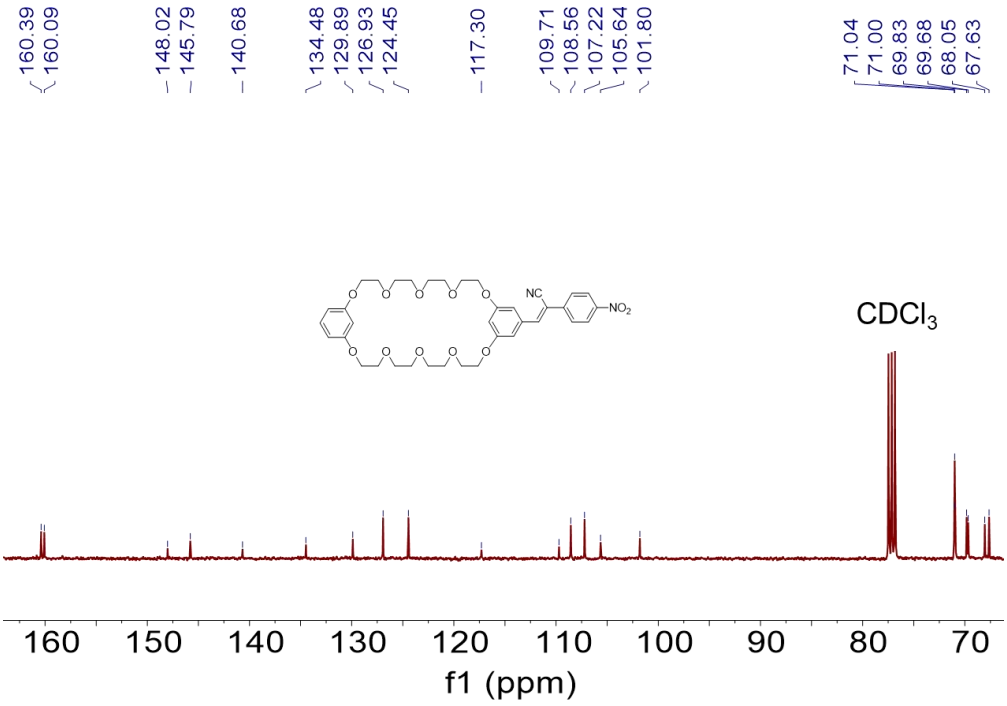

Fig. S2. The ^{13}C NMR spectrum (400 MHz, CD_3OD, 298 K) of **1**.

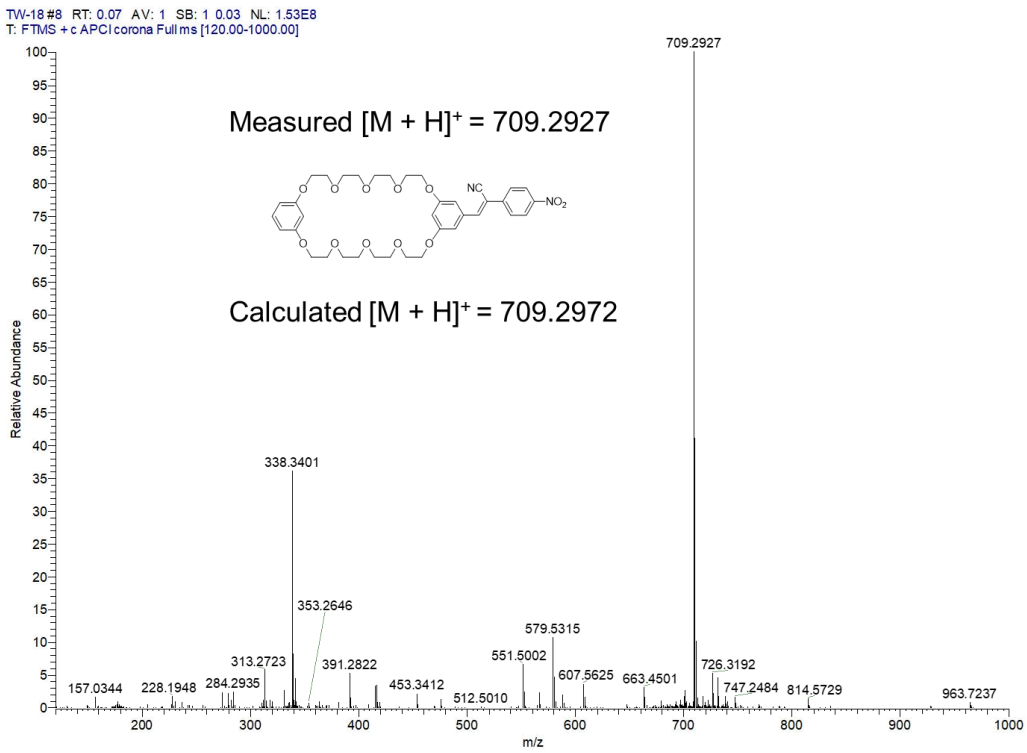

Fig. S3. The HRESI-MS of **1**.

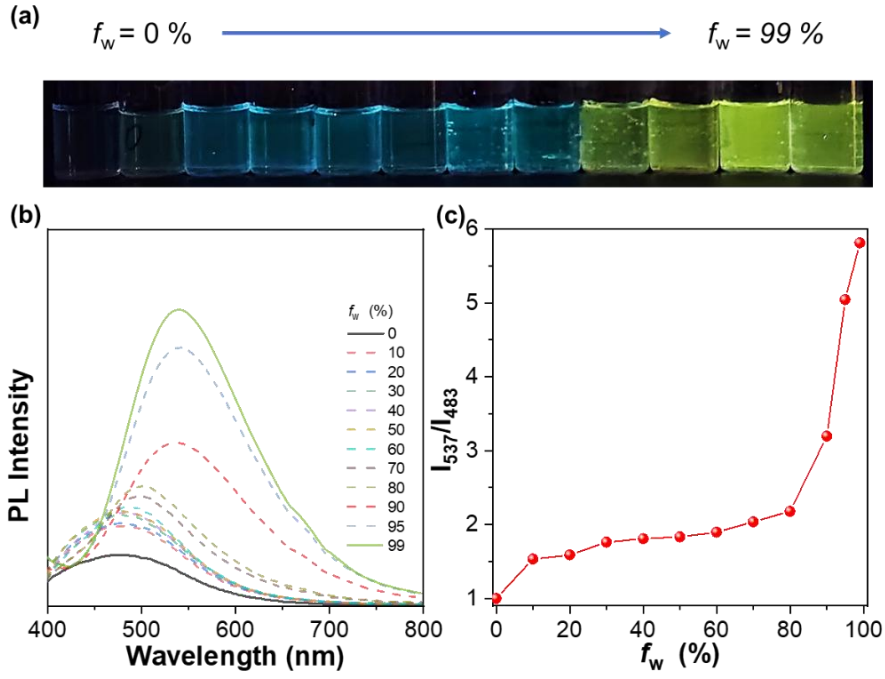

Fig. S4. (a) Photographs (λ_{ex} = 365 nm) and (b) PL spectra (λ_{ex} = 341 nm) of **1** in CH_3OH/H_2O mixture solution with different H_2O fractions (from 0 to 99%), under a concentration of $1.0 \times 10^{-}$

[5] M. f_w indicates the fraction value of water. (c) Plots of PL intensity ratio (I_{537}/I_{483}) of **1** with different H_2O fractions.

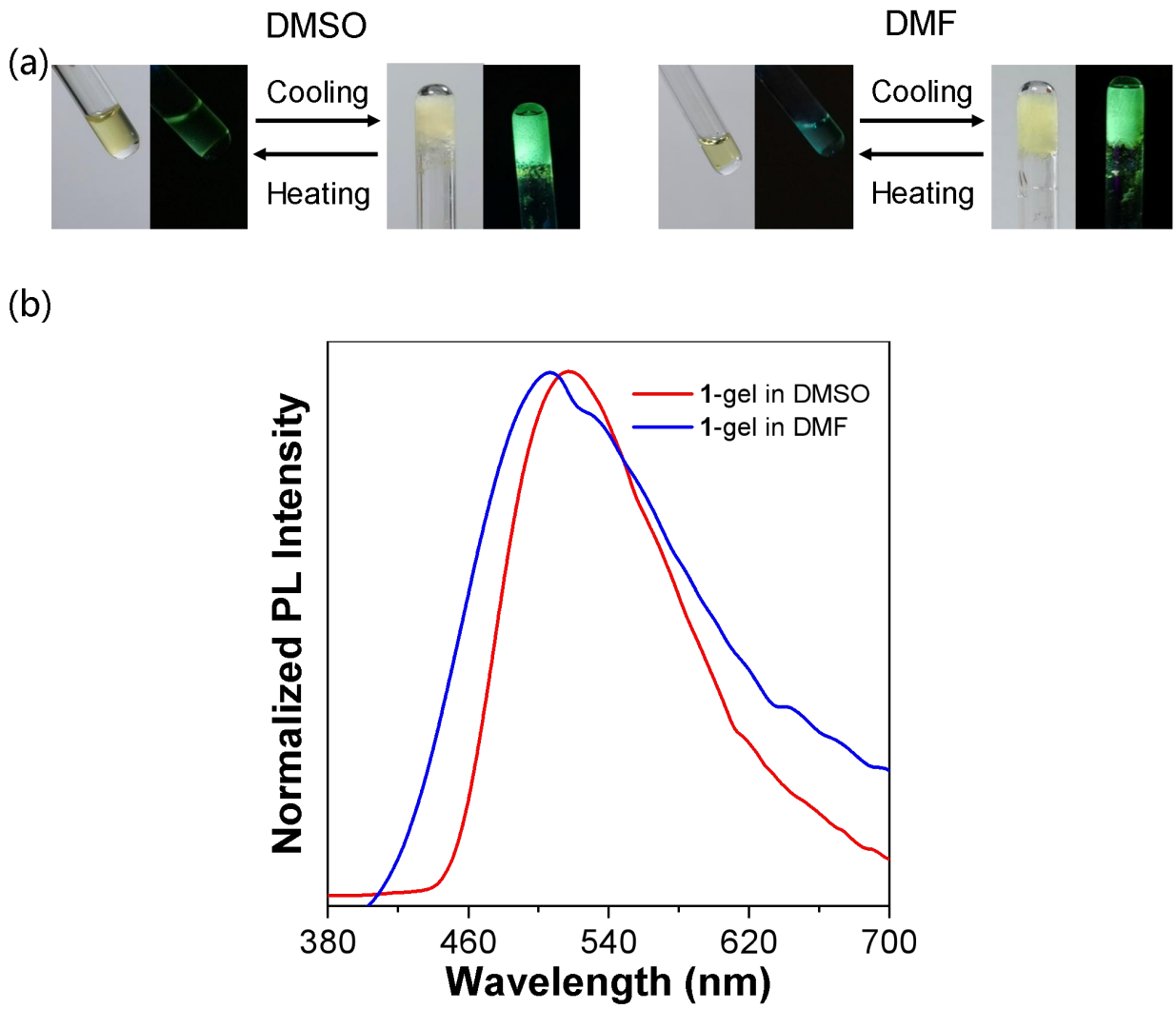

Fig. S5. Brightfield and PL photographs of thermal-induced gel-sol transition of **1** in (a) DMF and (b) DMSO solvents. (c) Normalized PL spectra of the gel **1** containing DMF and DMSO solvents (λ_{ex} = 341 nm).

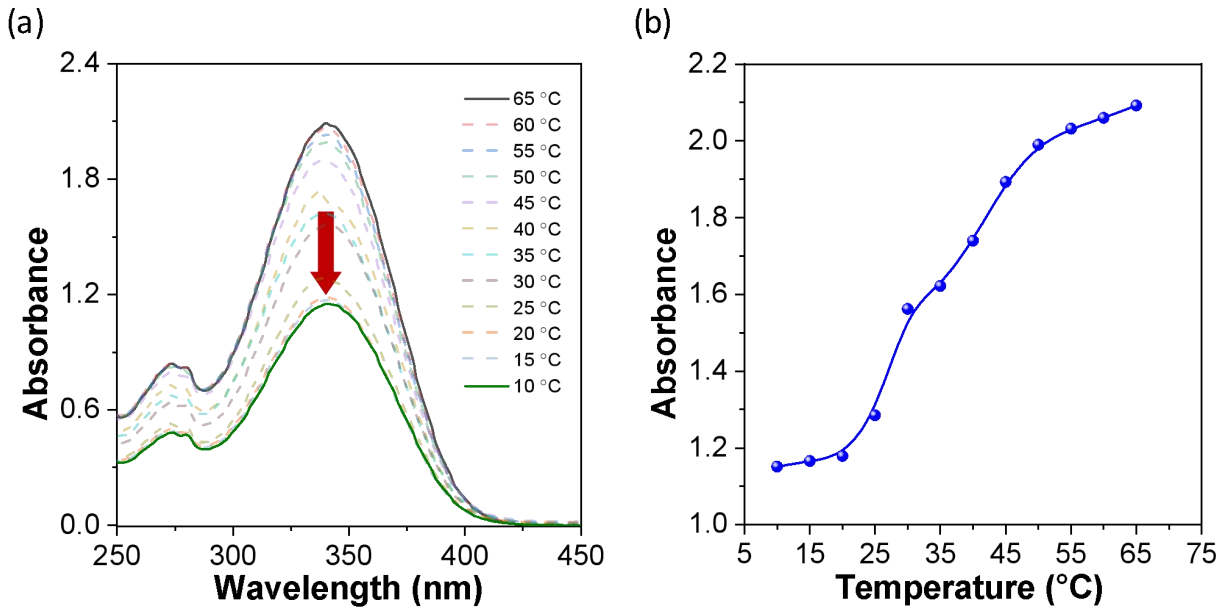

Fig. S6. (a) Temperature-dependent UV−vis absorption spectra of **1** in CH_3OH (10^{-5} M). (b) Plots of absorbance at 341 nm (a) at different temperature.

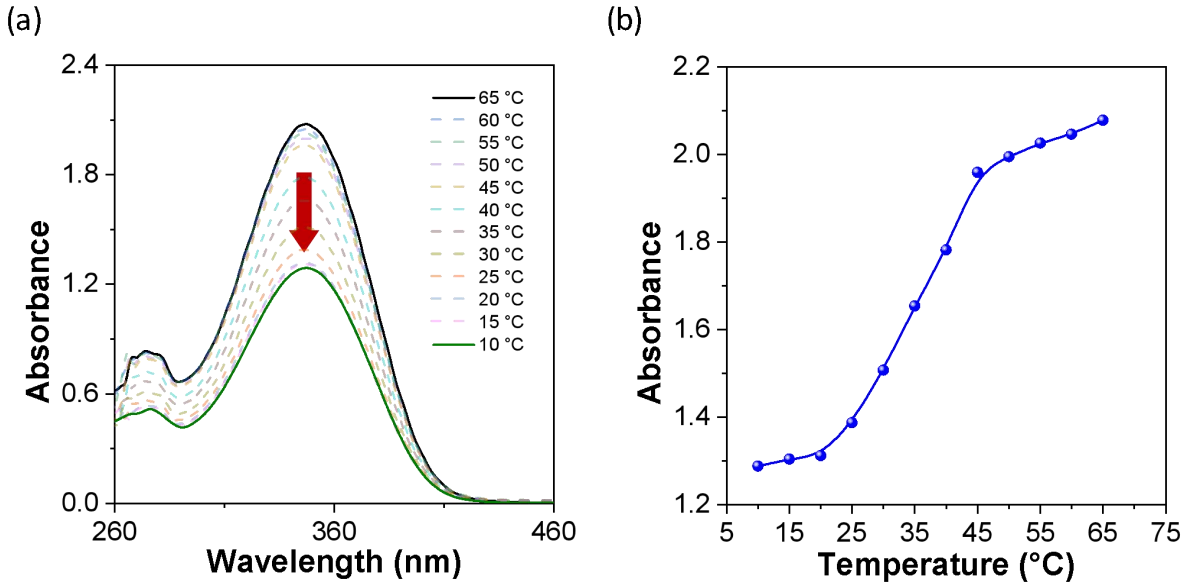

Fig. S7. (a) Temperature-dependent UV−vis absorption spectra of **1** in DMF (10^{-5} M). (b) Plots of absorbance at 347 nm (a) at different temperature.

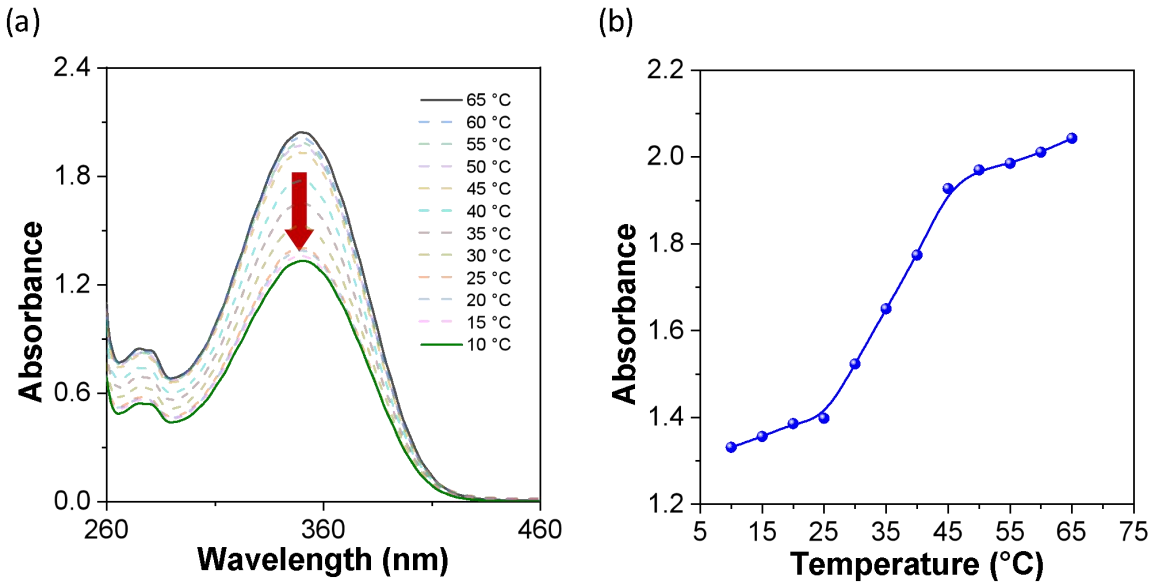

Fig. S8. (a) Temperature-dependent UV−vis absorption spectra of **1** in DMSO (10^{-5} M). (b) Plots of absorbance at 351 nm (a) at different temperature.

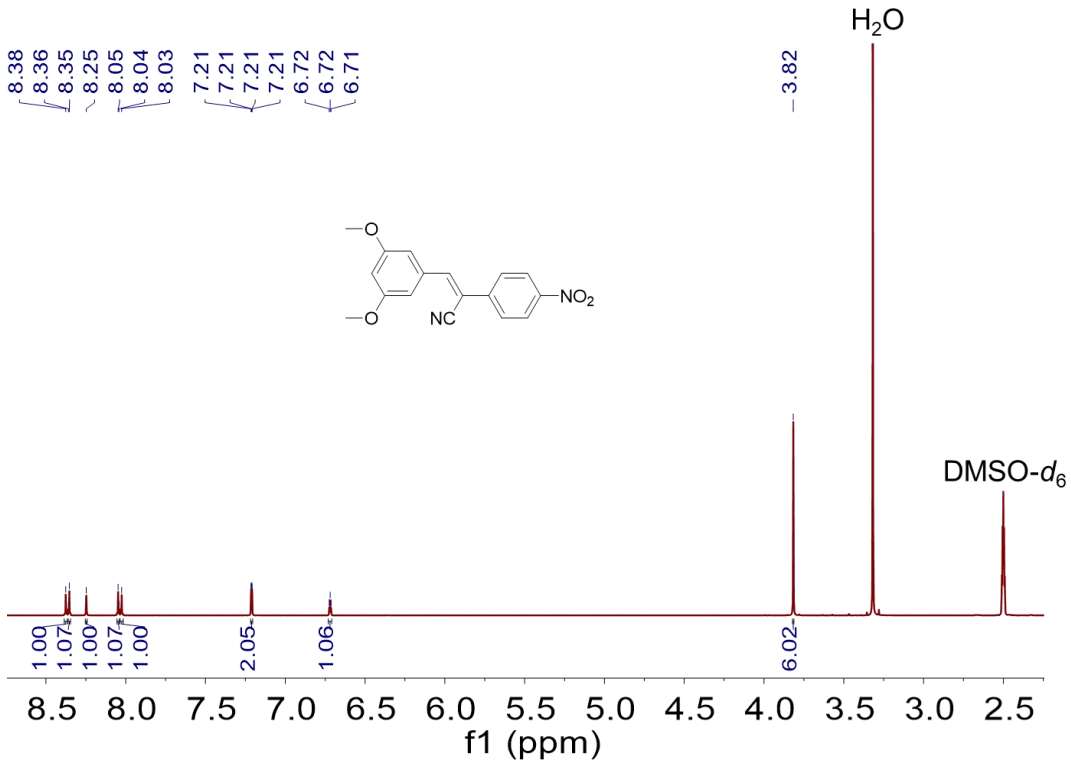

Fig. S9. The ^{1}H NMR spectrum (400 MHz, DMSO-d_6, 298 K) of M1.

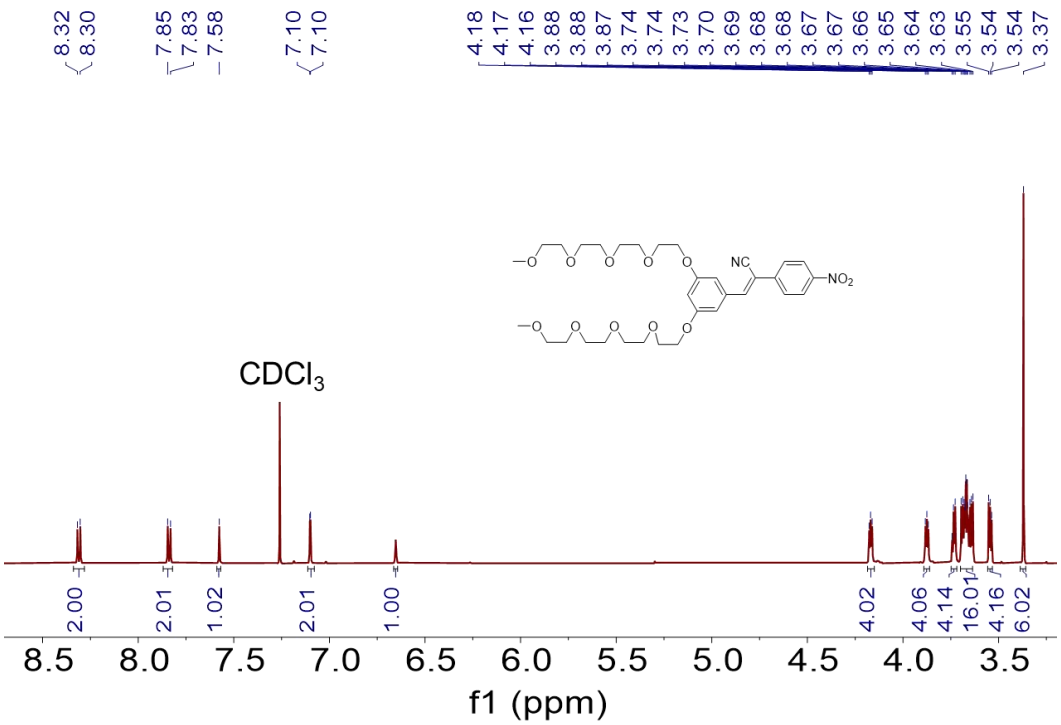

Fig. S10. The ^{1}H NMR spectrum (400 MHz, $CDCl_3$, 298 K) of M2.

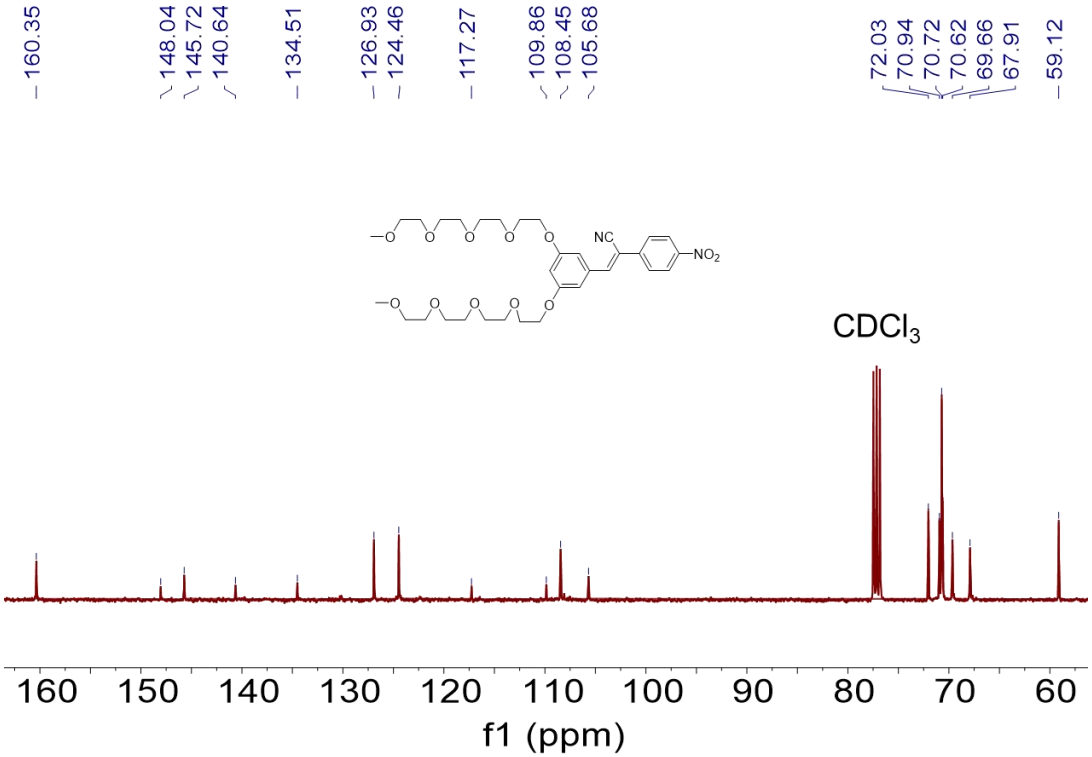

Fig. S11. The ^{13}C NMR spectrum (400 MHz, $CDCl_3$, 298 K) of M2.

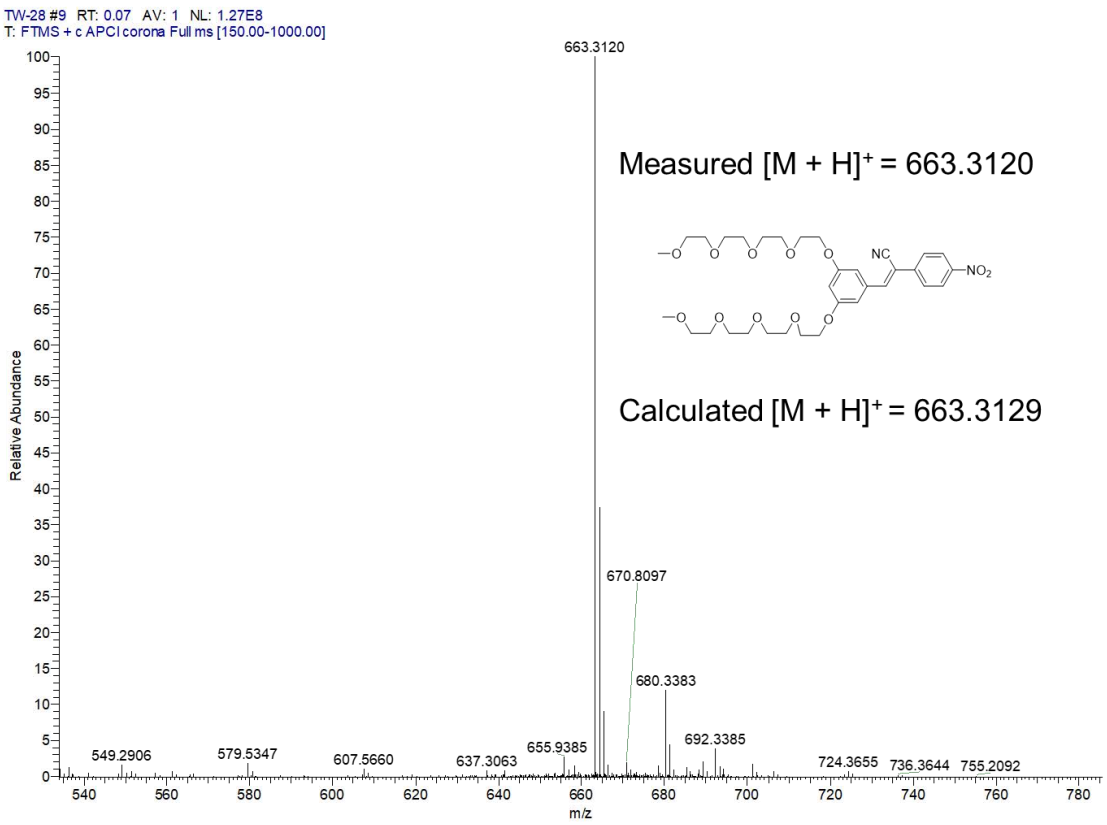

Fig. S12. The HRESI-MS of M2.

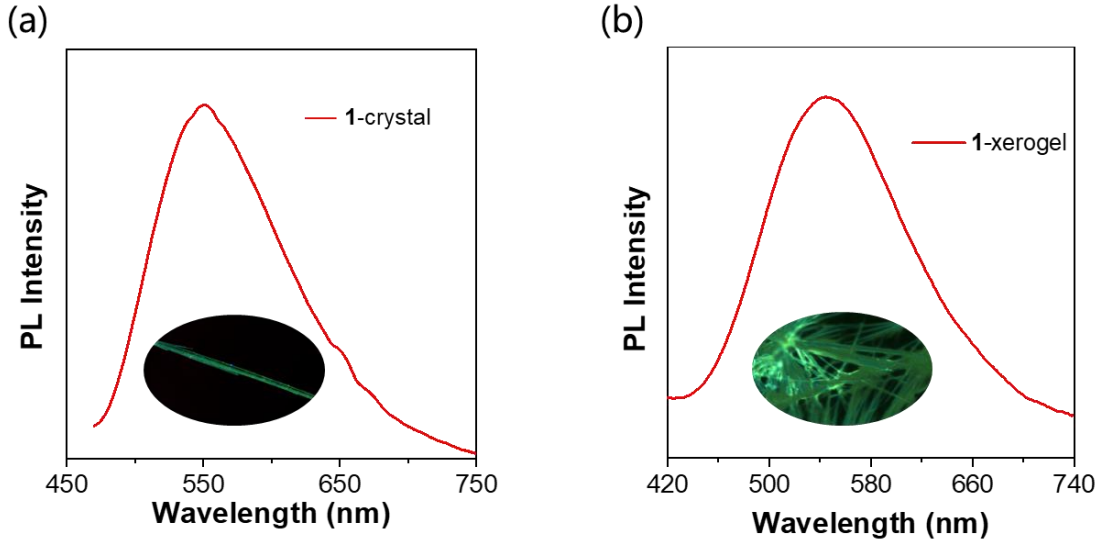

Fig. S13. PL spectra of (a) crystal **1** and (b) xerogel **1** at room temperature.

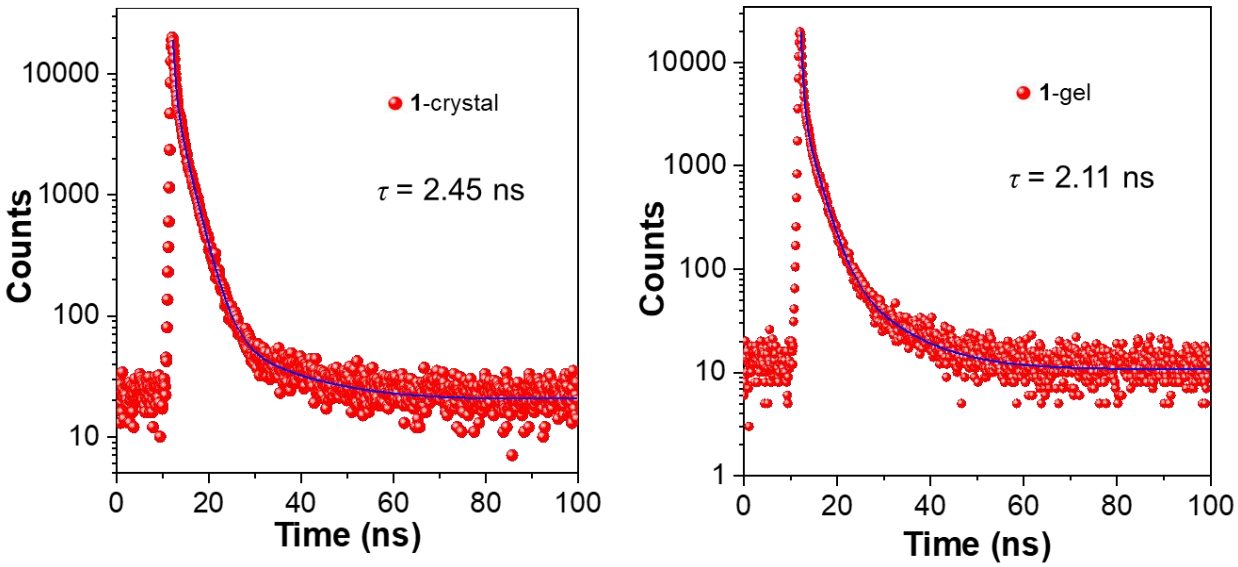

Fig. S14. Time-resolved emission decay curves of (a) crystal **1** and (b) xerogel **1** at room temperature.

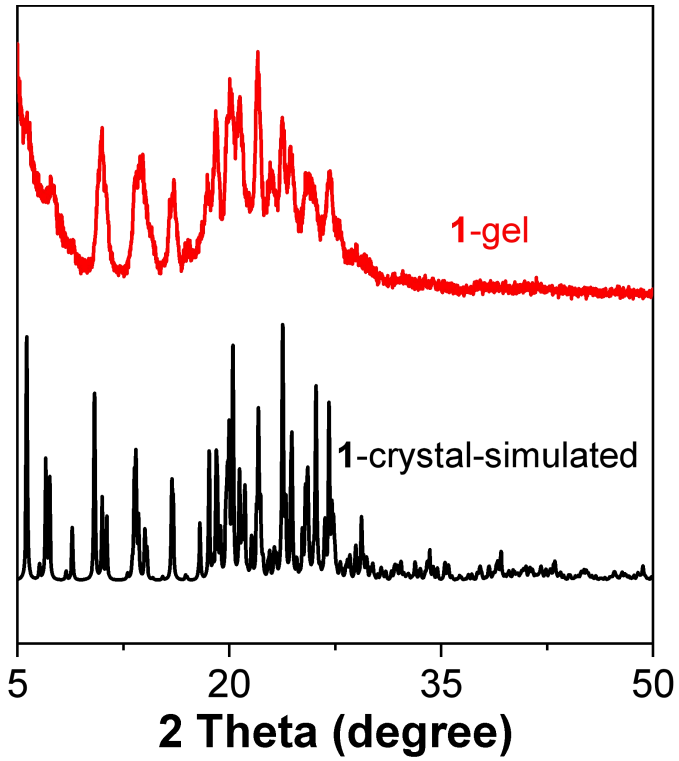

Fig. S15. Experimental powder XRD pattern of gel **1** and simulated XRD pattern of crystal **1**.

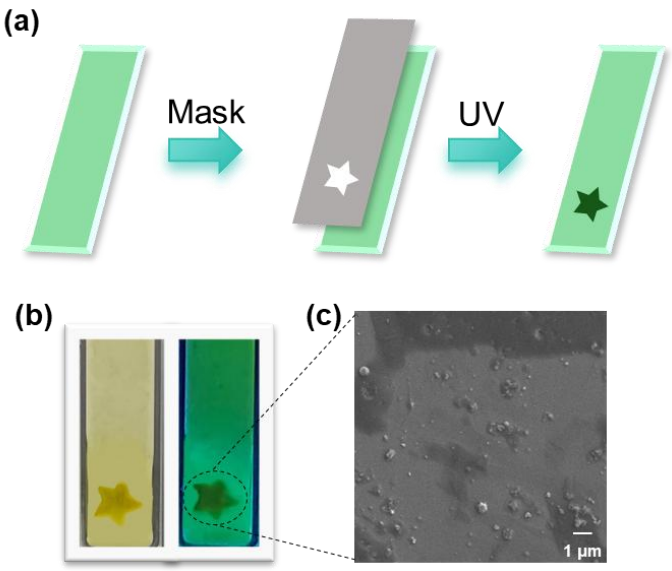

Fig. S16. (a) Scheme of the fluorescence pattern of gel **1** obtained under 365 nm UV irradiation through photomasks. (b) Brightfield and fluorescence images of the fluorescence pattern of gel **1** obtained after 365 nm UV irradiation through photomasks. (c) SEM image of xerogel obtained after 365 nm UV irradiation of gel **1**.

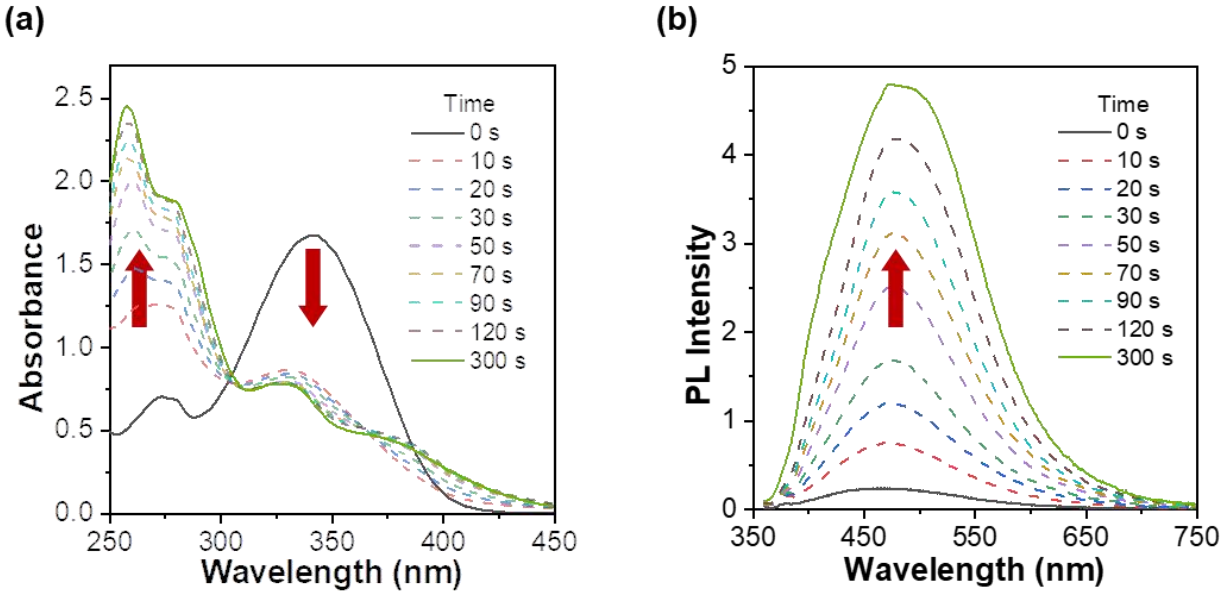

Fig. S17. Time-dependent (a) UV−vis absorption spectra and (b) PL spectra of **1** in CH_3OH (10^{-5} M) (λ_{ex} = 341 nm).

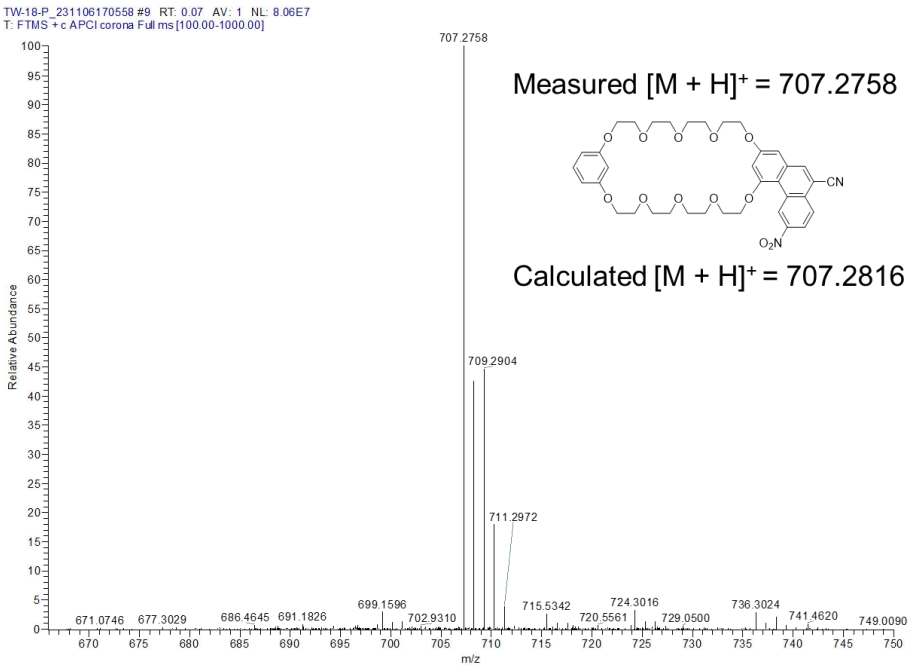

Fig. S18. The HRESI-MS of **1c**.

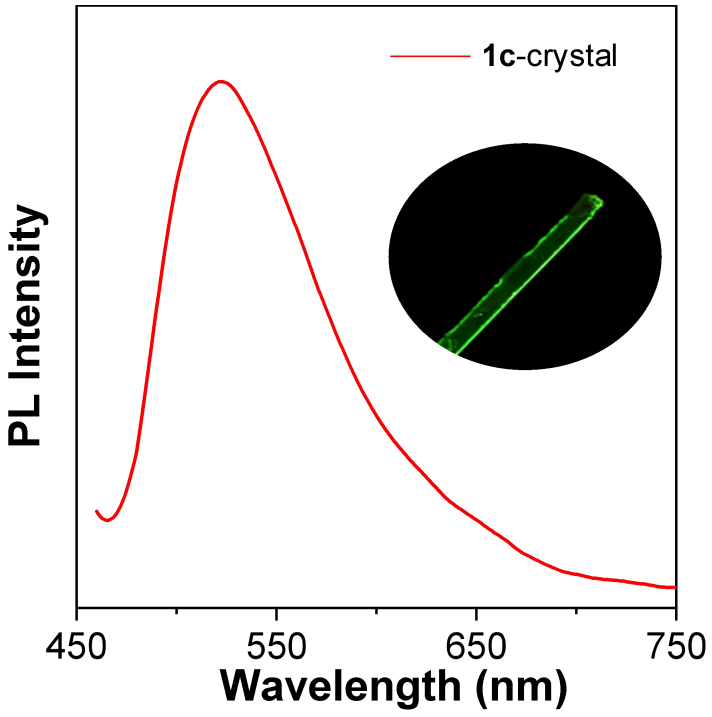

Fig. S19. PL spectrum of crystal **1c**. Inset is the fluorescent image of crystal **1c**.

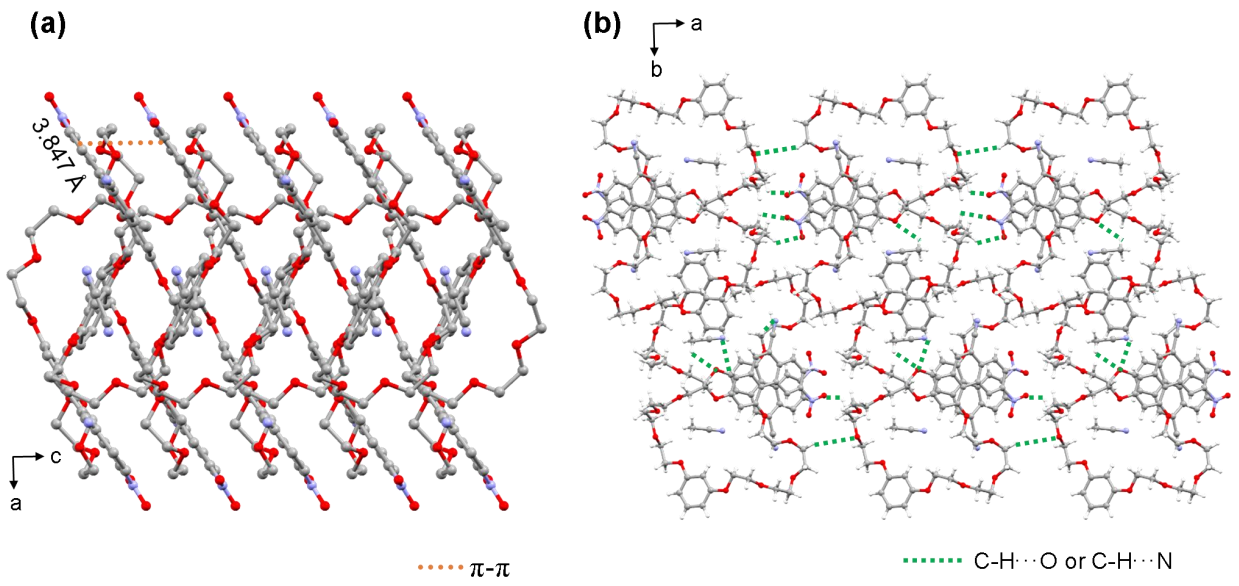

Fig. S20. (a) The packing structure and intermolecular interactions in crystals **1c**: orange dashed lines indicating π···π (distances 3.847 Å) interactions between adjacent molecules. (b) The intermolecular interactions in crystals **1c**: green dashed lines indicating C-H···O or C-H···N interactions between adjacent layers. Color code: gray, C; purple, N; red, O; white, H.

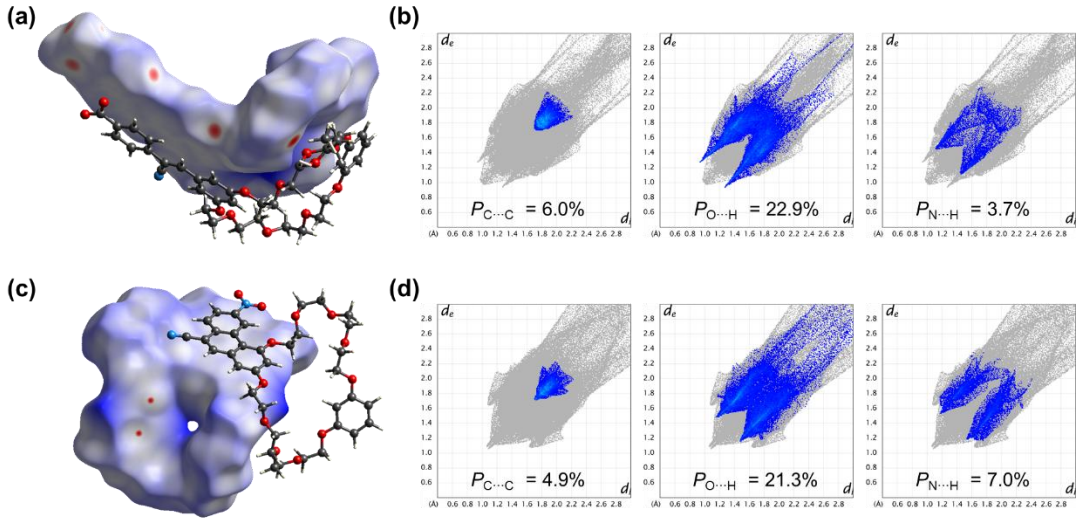

Fig. S21. Hirshfeld surface analysis (mapped over d_{norm}) based on (a) **1** and (c) **1c** crystal structures. Decomposed fingerprint plots of intermolecular C···C, O···H and N···H interactions based on (b) **1** and (d) **1c**. Full fingerprints appeared as grey shadows underneath decomposed plots, and selected intermolecular interactions were shown as a blue shadow.

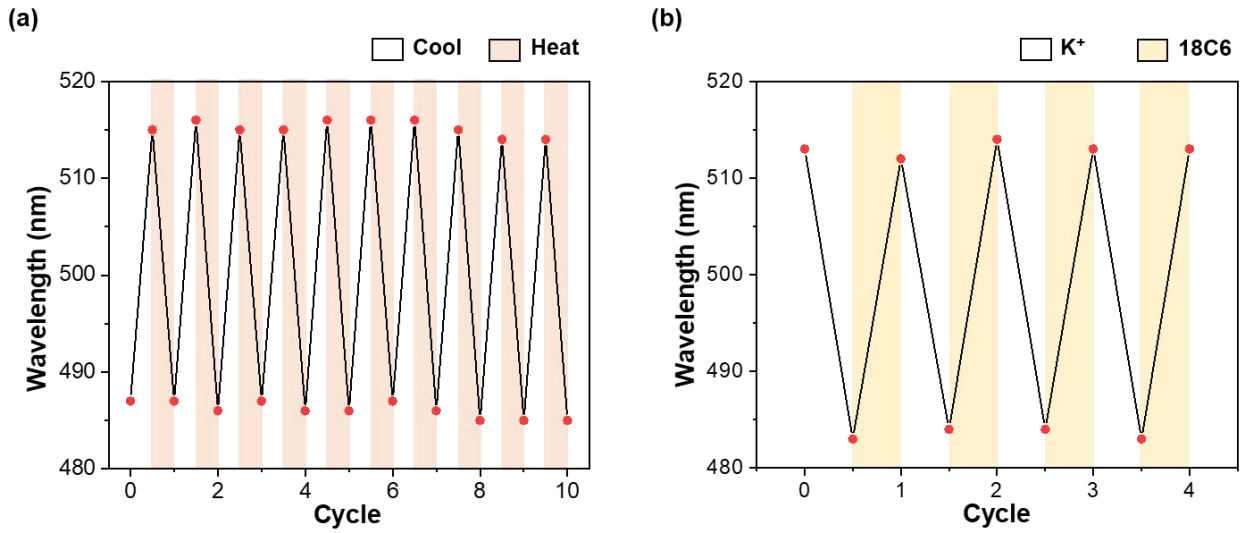

Fig. S22. (a) The emission peak changes of the gel **1** in CH_3OH with alternating cooling/heating cycles. (b) The emission peak changes of the gel **1** in CH_3OH with alternating adding K^+/18C6 cycles (λ_{ex} = 341 nm).

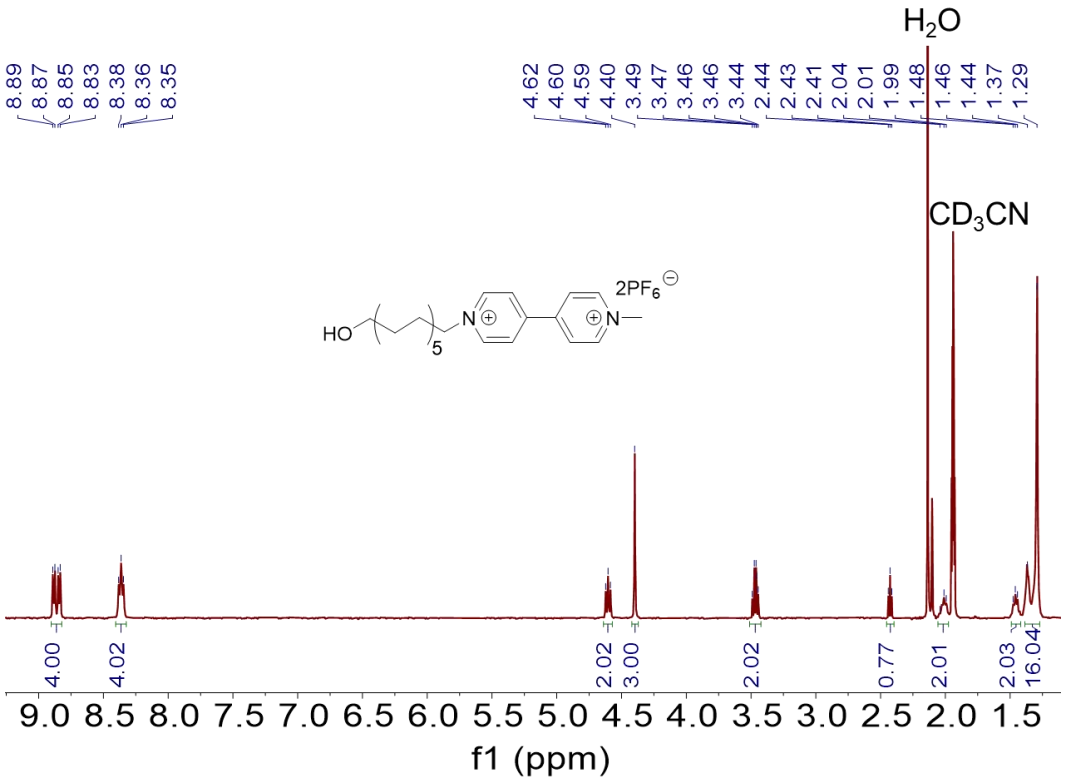

Fig. S23. The ^{1}H NMR spectrum (400 MHz, CD_3OD, 298 K) of PQD.

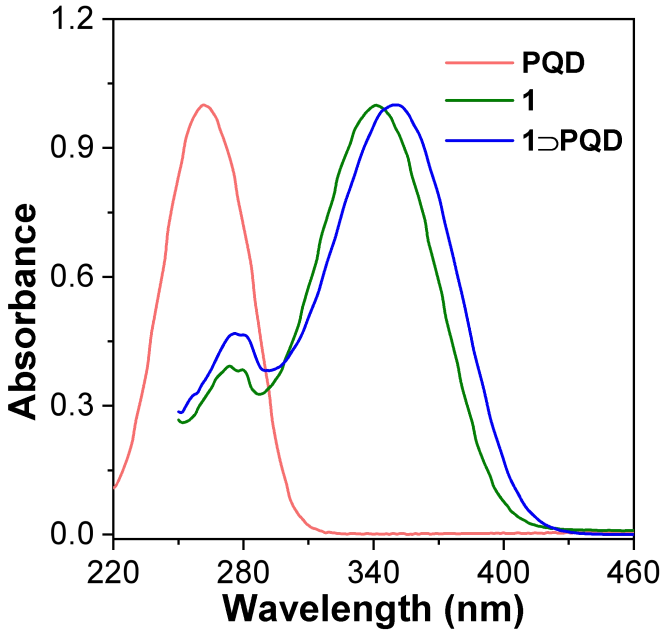

Fig. S24. The UV−vis absorption spectra of **1**, PQD and **1⊃PQD** in CH_3OH.

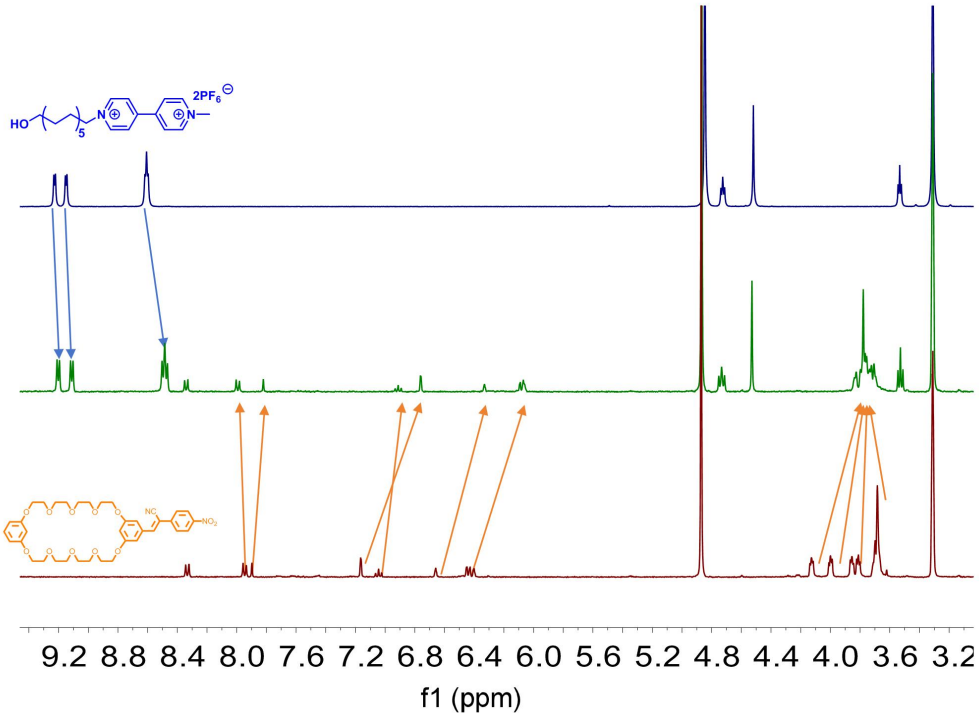

Fig. S25. The ^1H NMR spectra of **1**, PQD and **1⊃PQD** in CD_3OD.

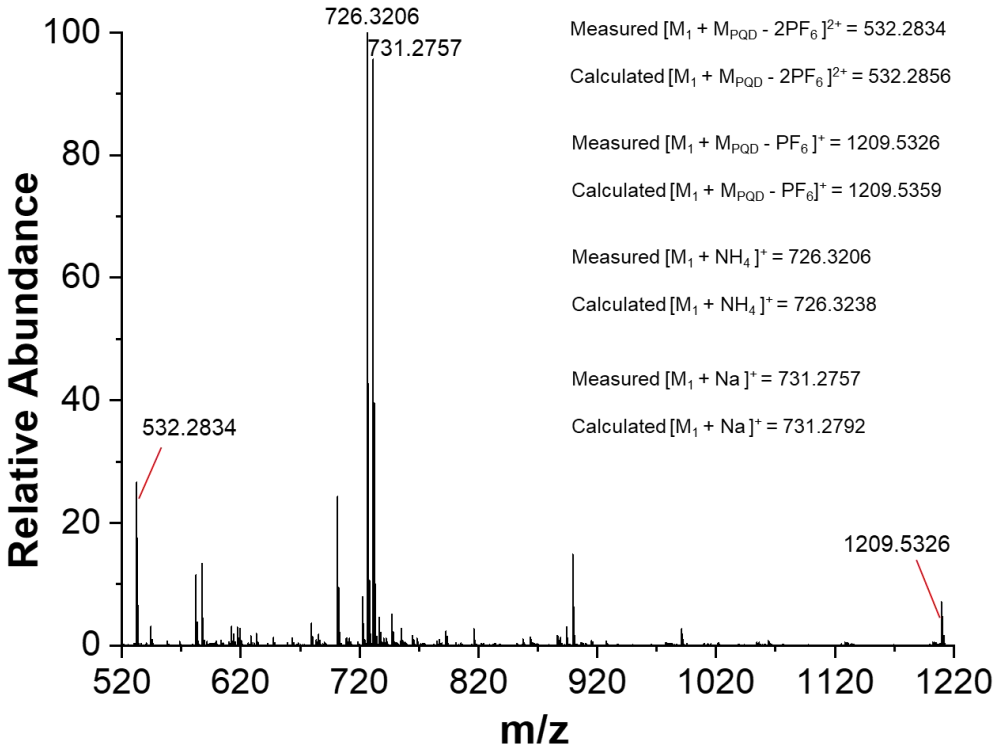

Fig. S26. The HRESI-MS of **1⊃PQD**.

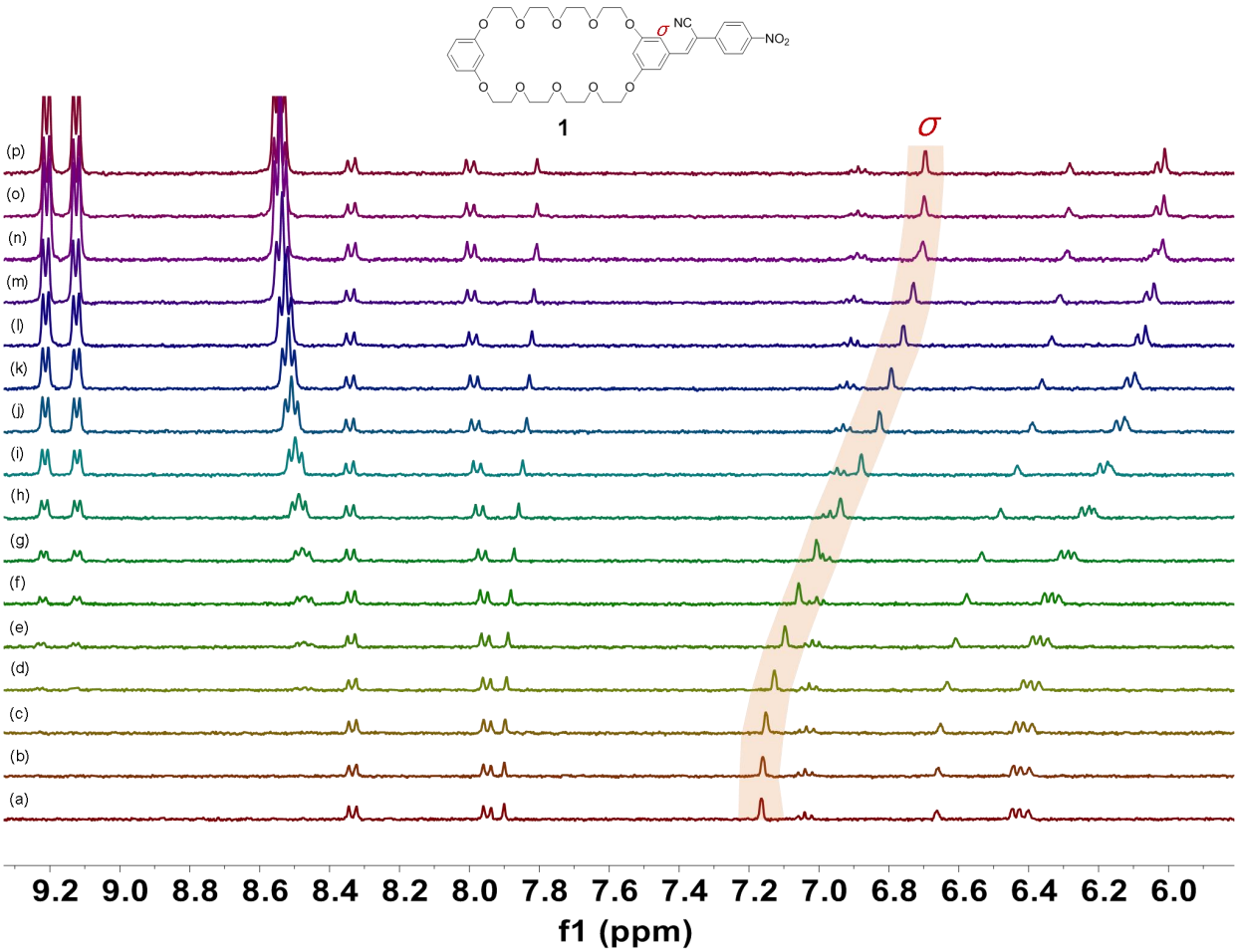

Fig. S27. ^{1}H NMR spectra (400 MHz, CD_3CN, 293 K) of **1** at a concentration of 1.00 mM with different concentrations of PQD: (a) 0.00 mM, (b) 0.04 mM, (c) 0.14 mM, (d) 0.33 mM, (e) 0.60 mM, (f) 0.86 mM, (g) 1.26 mM, (h) 1.83 mM, (i) 2.45 mM, (j) 3.17 mM, (k) 3.99 mM, (l) 4. 91mM, (m) 5.77 mM, (n) 6.63 mM, (o) 7.19 mM, (p) 7.48 mM.

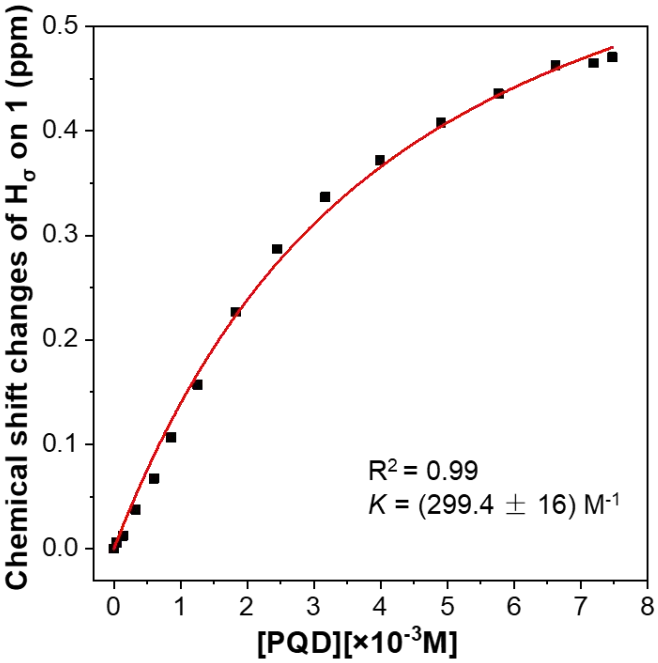

Fig. S28. The chemical shift changes of H_σ on **1** (1.00 mM) upon the addition of PQD with different concentrations. The red solid line was obtained from the non-linear curve-fitting using Eq. S1.

Fig. S29. Brightfield and fluorescent photographs of gel **1⊃PQD** (λ_{ex} = 365 nm).

Table S1 The gelation ability of **1** and **1⊃PQD** in organic solvents. G–gel; P–precipitate; S–soluble. *a1*: 1.73 wt%; *a2*: 2.46 wt%; *a3*: 2.53 wt%; *b*: 10.21 wt%.

Solvent	**1**	**1⊃PQD**	Solvent	**1**	**1⊃PQD**
THF	S	S	DMF	G[a2]	S
H_2O	P	P	DMSO	G[a3]	S
CH_2Cl_2	S	S	Acetone	S	S
$CHCl_3$	S	S	Acetonitrile	S	S
CH_3OH	G[a1]	G[b]	Ethyl acetate	S	P

Table S2 Crystal data and structure refinement for **1** and **1c**.

Crystal	**1**	**1c**
Empirical formula	$C_{37}H_{41}N_2O_{12}$	$C_{39}H_{45}N_3O_{12}$
Formula weight	705.72	747.78
Temperature/K	120	120
Crystal system	monoclinic	monoclinic
Space group	*P 21/c*	*P 21/c*
a/Å	31.3061	16.1387
b/Å	4.7010	28.3321
c/Å	26.9834	8.3321
α/°	90	90
β/°	93.029	95.419
γ/°	90	90
Volume/Å^3	3965.6	3792.8
Z	4	4
ρ_{calc}/g cm^{-3}	1.182	1.310
μ/mm^{-1}	0.741	0.812
F(000)	1492.0	1584.0
R_1/%	9.76	9.92
CCDC number	2360348	2360343

Reference

1 P. Wei, X. Zhang, J. Liu, G.-G. Shan, H. Zhang, J. Qi, W. Zhao, H. H. Y. Sung, I. D. Williams, J. W. Y. Lam and B. Z. Tang, *Angew. Chem. Int. Ed.*, 2020, **59**, 9293-9298.

2 X. Zhang, J. Gong, W. Tao, X. Jiang, C. Chen and P. Wei, *ACS Mater. Lett.*, 2022, **4**, 1468-1474.

3 T. T. K. Cuc, C.-H. Hung, T.-C. Wu, P. Q. Nhien, T. M. Khang, B. T. B. Hue, W.-T. Chuang and H.-C. Lin, *Chem. Eng. J.*, 2024, **485**, 149694.